Site location and crystal field of Nd^{3+} ions in congruent strontium barium niobate

P. Molina,[1] H. Loro,[2] S. Álvarez-García,[1,*] L. E. Bausá,[1] E. Martín Rodriguez,[1] O. Guillot-Noël,[3,†] Ph. Goldner,[3] M. Bettinelli,[4] P. Ghigna,[5] and J. García Solé[1]

[1]*Dpto. Física de Materiales, Universidad Autónoma de Madrid, Campus de Cantoblanco, E-28049 Madrid, Spain*

[2]*Facultad de Ciencias, Universidad Nacional de Ingeniería, P.O. Box 31-139, Lima, Peru*

[3]*Laboratoire de Chimie de la Matière Condensée de Paris UMR-CNRS 7574, Ecole Nationale Supérieure de Chimie de Paris, 11 rue Pierre et Marie Curie, 75231 Paris Cedex 05, France*

[4]*Laboratorio d'Chimica dello Stato Solido, DB, Università di Verona, and INSTM, UdR Verona, Strada Le Grazie 15, I-37314 Verona, Italy*

[5]*Dipartimento di Chimica Fisica "M. Rolla," Università di Pavia, Viale Taramelli 16, I-27100 Pavia, Italy*

(Received 13 May 2009; revised manuscript received 20 July 2009; published 31 August 2009)

The site location of Nd^{3+} ions in congruent strontium barium niobate ($Sr_{0.6}Ba_{0.4}Nb_2O_6$) has been systematically investigated by means of low-temperature optical and electron paramagnetic resonance spectroscopies. The experimental results obtained by these complementary techniques clearly indicate that Nd^{3+} ions are mainly located in only one of the four available cationic sites, the A2 sites, and preserving the C_s local symmetry of these host cation sites. The energy levels and g-factor value experimentally obtained by both techniques have been used to calculate the crystal field parameters for the Nd^{3+} ions in this A2 cationic site.

DOI: 10.1103/PhysRevB.80.054111 PACS number(s): 61.72.U−, 78.30.−j, 76.30.Kg, 71.55.−i

I. INTRODUCTION

Strontium barium niobate, $Sr_xBa_{1-x}Nb_2O_6$ (abbreviated SBN), is a fascinating family of ferroelectric mixed crystals with a great number of potential applications in photonics, such as optical data storage, switching, and optical computing.[1–4] SBN has been recently considered as a "nonlinear photonic glass," as it is able to produce multidirectional second and third harmonic generation for a variety of geometries and in a broad spectral range.[5] Moreover, SBN can be easily doped with optical active ions leading to solid state lasers which can display a variety of additional functions, such as self-frequency conversion (self-frequency doubling and self-frequency sum),[6] tunability,[7] and, more recently, bistable laser output.[8,9] This last feature is based on the relatively low Curie temperature of SBN crystals, which allows that the phase transition can be driven by means of pump power induced thermal changes. In addition, the phase transition temperature depends on both host stoichiometry (i.e., on x, $0.25 \leq x \leq 0.75$)[1,10] and on the doping ions and their concentration.[11–13]

It has been recently shown that the luminescence of Nd^{3+} ions in congruent ($x=0.6$) SBN crystal is almost insensitive to phase transition, while that of Tm^{3+} and Yb^{3+} ions is highly sensitive to temperature changes around the Curie temperature.[14] This different spectral sensitivity of the rare-earth ions to the phase transition was proposed to be related to the different distribution of the rare earth ions among the available cationic sites in the ferroelectric SBN crystal host.[14]

The general formula of SBN can be written as $(A_1)_4(A_2)_2(B_1)_2(B_2)_8O_{30}$, the space group at room temperature being $P4bm$,[15–18] so that four different cationic sites can be in principle occupied by the Nd^{3+} ions. Figure 1 show a part of the SBN structure (at room temperature) viewed along the ferroelectric c axis and displaying the available cationic sites. (i) The A1 sites (C_4 symmetry and 12-fold coordination), which are partially occupied by Sr^{2+} ions; (ii) the A2 sites (C_s symmetry and 15-fold coordination), in which the Sr^{2+} and Ba^{2+} host cations are distributed in a disordered way to partially fill these sites; (iii) the B sites, which are completely filled by the Nb^{5+} sublattice, and occur in two different local symmetries, the B1 sites (C_{2v} symmetry) and the B2 sites (C_1 symmetry), both being distorted octahedral sites (sixfold coordination). Thus, by means of site selective spectroscopy it has been recently shown that Yb^{3+} ions are occupying the four available A and B cationic sites in ferroelectric SBN (the phase present at room temperature).[19,20] The lattice location of Eu^{3+} ions has been also investigated in congruent SBN crystals grown by different methods.[13,21] It seems that the growth method affects the site location of these ions: while in SBN crystals slowly grown at high temperatures by using the Czochralski technique the B octahedral sites seems to be favored,[13] in SBN

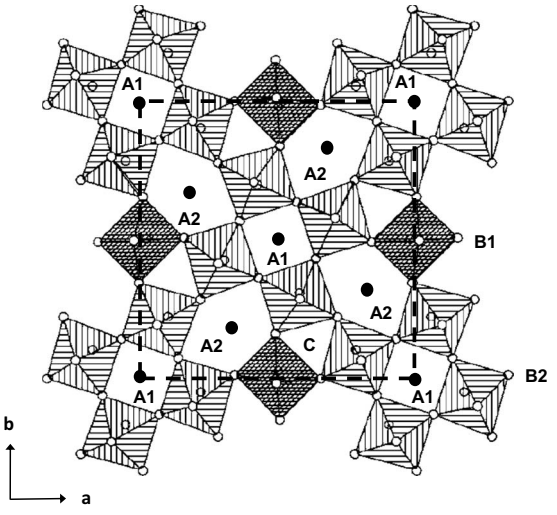

FIG. 1. Projection of part of the SBN structure viewed along the c axis

crystals grown at lower temperatures by spontaneous nucleation in a flux the Eu^{3+} ions seem to occupy mainly the A1 site.

However, in spite of the importance of the Nd^{3+} ions as laser active centers, there is no information about the location of these ions in the SBN host, so that this is still an open question. This aspect is essential in order to understand the relevant spectroscopic and laser properties of this ion in the SBN crystal and therefore tailoring optical devices based on SBN:Nd.

In this work we present a detailed investigation to determine the site location of Nd^{3+} ions in congruent ($x=0.6$) SBN crystals. For this purpose we have used two experimental techniques based in different spectral ranges of the electromagnetic spectrum, optical spectroscopy, and electron paramagnetic resonance (EPR). Optical spectroscopy studies include the so-called total site selective spectroscopy (TSSS), which is quite useful to determine the number of different nonequivalent environments for the Nd^{3+} ions (Nd centers). Moreover the polarization character of the absorption (excitation)/emission lines of each individual center can be used to determine its site symmetry. EPR spectroscopy is a powerful tool to identify paramagnetic ions, such as Nd^{3+}, in different sites. The g factor of a paramagnetic ion is closely related to the wave function of the electronic ground state and therefore depends not only on the spin-orbit coupling but also on the point symmetry of the crystallographic site. The sensitivity of EPR to local symmetry is such that ions in sites with slightly different symmetries give EPR spectra with well distinct resonance lines.

The experimental results obtained by both techniques unequivocally reveal that Nd^{3+} ions are mainly occupying the A2 site. Thus, once this location has been evidenced, the low-temperature optical (absorption and emission) spectra have been used to identify the majority of the Stark energy levels. Then a Hamiltonian including the Coulomb spin-orbit interconfigurational interaction terms of the Nd^{3+} ($4f^3$) configuration and crystal field terms of C_s symmetry (A2 site) was used to fit these energy levels.

II. EXPERIMENTAL DETAILS

A single congruent SBN ($x=0.6$) crystal doped with a 1% of Nd^{3+} ions (with respect to Nb^{5+}) was grown by the Czochralski technique. The samples were cut with the c axis parallel or perpendicular to the main face in order to perform polarized optical measurements and EPR experiments.

Polarized optical absorption measurements were carried out from the UV to the infrared spectral range by means of a U-1050 Perking Elmer spectrophotometer. For the low temperature absorption measurements (10 K) a closed cycle cryostat was used. TSSS measurements were made at 10 K by using a liquid He cryostat and exciting with an Ar^+ pumped continuous-wave Ti:Sapphire laser (Spectra Physics 3900), which was used as a tunable source. The emitted light was directed into a double-grating monochromator and then detected by a calibrated Ge detector.

EPR measurements were performed at 10 K with a X-band (9.5 GHz) Bruker ELEXSYS E 500 spectrometer, equipped with a variable temperature accessory from Oxford instrument. The crystals were mounted on a small Perspex sample holder to allow their orientation with respect to the magnetic field. The determination of the principal g values, namely, g_x, g_y, and g_z, was obtained from the angular variations of the experimental g factor in three orthogonal crystal planes, e.g., the crystallographic (ab), (bc), and (ac) planes. These angular variations were obtained by rotating the crystal by steps of 10° around reference axes with ≈2° accuracy for crystal orientation.

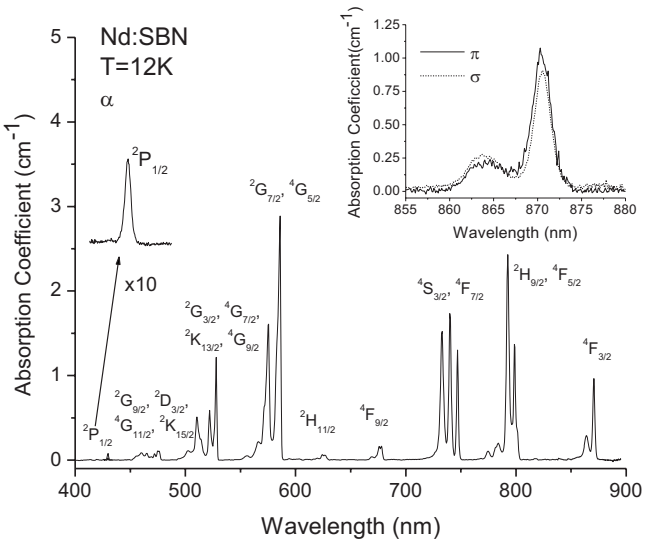

FIG. 2. (a) Absorption spectrum (12 K) in α polarization. The inset in the right side shows the σ and π polarized spectra in the spectral range corresponding to ${}^4I_{9/2} \rightarrow {}^4F_{3/2}$ transition. Notice (left side) that the ${}^4I_{9/2} \rightarrow {}^2P_{1/2}$ transition has been magnified by a factor of 10.

III. EXPERIMENTAL RESULTS AND DISCUSSION

A. Nd^{3+} ions site symmetry location

1. Optical spectroscopy

Figure 2 shows the 12 K absorption spectrum of Nd^{3+} in SBN in α polarization, i.e., with the beam parallel to the ferroelectric c axis. This spectrum consists of groups of lines corresponding to transitions between the lowest Stark energy level of the ground (${}^4I_{9/2}$) state to Stark energy levels belonging to different ${}^{2S+1}L_J$ excited states (where S, L, and J are the spin-orbital and total-angular momenta) inside the $4f^3$ electronic configuration of the free Nd^{3+} ion. The involved ${}^{2S+1}L_J$ excited states have been indicated in the figure. This absorption spectrum has also been recorded in σ polarization (beam and electric field perpendicular to c axis) and π polarization (beam perpendicular to c axis and electric field parallel to c axis) but these spectra are not included in the figure for the sake of simplicity. Nevertheless the inset shows σ and π polarized spectra in the particular wavelength range 850–880 nm, where excitation has been performed in this work. These spectra are associated with the transitions from the lowest Stark sublevel (level 1, at 0 cm^{-1}) of the ground ${}^4I_{9/2}$ state up to the two Stark sublevels of the ${}^4F_{3/2}$ excited

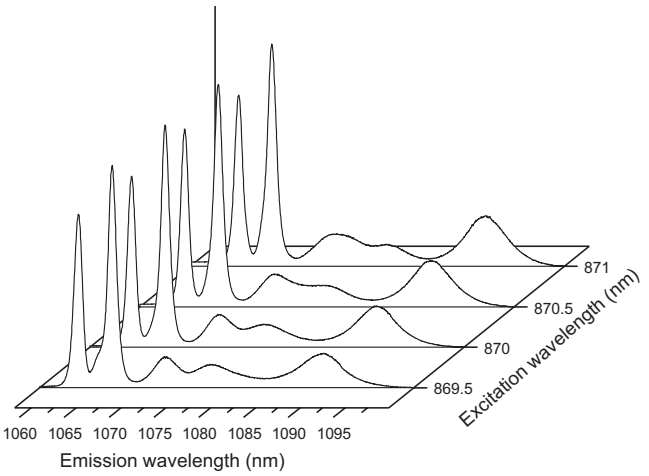

FIG. 3. Unpolarized site selective emission spectra (10 K).

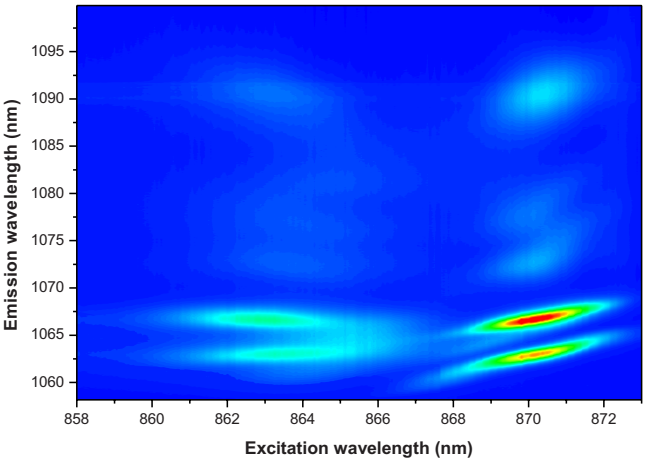

FIG. 4. (Color online) Contour plot of the total site selective spectrum of $^4I_{9/2} \rightarrow R_1$, R_2 excitations, and $R_1 \rightarrow 1(^4I_{11/2})$ emission.

state. These levels are usually labeled as R_1 and R_2, in order of increasing energy, and so the two observed peaks, at around 864 and 871 nm, respectively, correspond to the $1 \rightarrow R_2$, R_1 electronic transitions. As observed these two transitions appear in both σ and π polarizations although with different intensities. This is the trend generally observed: all observed interStark transitions appear (are allowed) for both polarizations. Moreover, the σ and α spectra are coincident, which indicates the electric dipole nature of the Nd^{3+} transitions in SBN.

At this point it is important to mention that in all four available lattice cation sites for Nd^{3+} ions in SBN, the $^4F_{3/2}$ excited state should split into two levels (R_1 and R_2). Thus, the absence of other bands suggests that the observed spectrum essentially corresponds to a unique main site occupied by the Nd^{3+} ions. In fact the absence of other structure is also manifested in the low temperature $^4I_{9/2} \rightarrow {}^2P_{1/2}$ absorption peak at 429.7 nm, which has been magnified in Fig. 2 for the sake of clarity. It should be also noted a large inhomogeneous broadening of this absorption band (full width at half maximum of 38 cm^{-1}) which, as commented below, is due to a large disorder in the SBN host.

The above results confirm that Nd^{3+} ions are mainly accommodated in one lattice site. In order to confirm this hypothesis and so gain additional information on the main SBN host lattice site replaced by the Nd^{3+} ions, detailed TSSS experiments have been carried out.

The most intense emission spectrum of Nd^{3+} ions in crystals originates from the $^4F_{3/2}$ metastable state to the lower lying ^4I_J states. Figure 3 shows four 10 K emission spectra corresponding to the $^4F_{3/2} \rightarrow {}^4I_{11/2}$ channel, excited at four different close laser wavelengths around the $1 \rightarrow R_1$ absorption (excitation) peak. It can be clearly appreciated that the peak positions and widths of the emission bands are unaffected by the excitation wavelength, this fact corroborating that the absorption spectrum of Nd^{3+} ions in SBN is related to a main single center (site). Moreover, in order to confirm this aspect, TSSS was systematically investigated in the excitation/emission spectral range involving the $^4I_{9/2} \rightarrow R_1R_2/R_1 \rightarrow {}^4I_{11/2}$ transitions. Figure 4 shows the spectroscopic maps in the excitation wavelength range from 858 to 872 nm ($^4I_{9/2} \rightarrow R_1R_2$ transitions) and in the emission range from 1060 to 1090 nm ($R_1 \rightarrow {}^4I_{11/2}$ transitions). The different slope observed in the TSSS maps of Fig. 4 in the region of the $R1$ and $R2$ transitions is related to the different shape of the $R1$ and $R2$ lines. In general, in most of Nd^{3+} doped compounds the spectral shape of the $R2$ line at low temperature exhibits a rather complicated structure, being much broader than the $R1$ line as a result of fast nonradiative decay. This is also our case. The broadening of the $R2$ line masks the inhomogeneous broadening of Nd^{3+} ions and, accordingly, no slope is observed on the spectral map in the region of that band. Opposite, at low temperature the $R1$ line is not affected by nonradiative decay and it is more suitable to demonstrate the presence of the different possible sites or just the inhomogeneous broadening through the slope in the excitation/emission map contour plot. In our case, a detailed inspection of that plot reveals a strong inhomogenous broadening but a single structure around the different excitation/emission transitions. This fact confirms the presence of a single Nd^{3+} center, i.e., a dominant site occupied by the Nd^{3+} ions.

In order to determine the occupied site, the local symmetry around Nd^{3+} ions in the observed center has been studied by means of polarized luminescence. Figure 5 shows the 10 K $^4F_{3/2} \rightarrow {}^4I_{11/2}$ emission spectra of the detected site for the σ and π configurations. As observed in optical absorption, the σ emission spectrum is the same the α one (not displayed for the sake of brevity), which again indicates the electric dipole (ED) nature for the Nd^{3+} transitions. Figure 5 reveals also the appearance of the same peaks (at least five) in both polarization configurations but with different relative intensities. Therefore we can say that all the observed transitions are sensitive to polarization and display σ and π character.

Let us now discuss on the possible occupied site. For this purpose we consider the results obtained for the $^4F_{3/2} \rightarrow {}^4I_{11/2}$ transitions, but the same conclusions can be drawn by means of other transitions involving different $^{2S+1}L_J$ states. For Nd^{3+} ions located in any of the four available sites (local symmetries) the degeneracy of the excited ($^4F_{3/2}$) and ground ($^4I_{9/2}$) states, responsible for the emission spectra in Fig. 5, should be completely lifted except for the Kramers

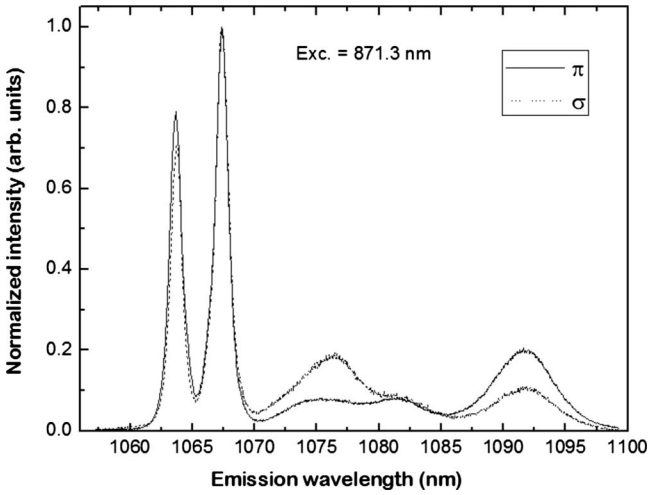

FIG. 5. $^4F_{3/2} \rightarrow {}^4I_{31/2}$ polarized emission spectra (10 K, excitation at 871.3 nm).

degeneracy. Thus, we should expect six peaks, at variance with the five that are observed. In fact, the above mentioned cationic disorder, together with a certain disorder on the anionic (oxygen) sublattice of SBN (Ref. 22) produce optical bands with a strong inhomogeneous broadening for the rare earth ions,[13,14,19,23–25] as commented above for the $^4I_{9/2} \rightarrow {}^2P_{1/2}$ transition of Nd^{3+} ions (see inset in Fig. 2). This inhomogeneous broadening is very likely responsible for the fact that one of the Stark components is not resolved in the (R_1) $^4F_{3/2} \rightarrow {}^4I_{11/2}$ emission spectrum.

Table I reports the irreducible representations of the split components which are expected for the $^4F_{3/2}$ and $^4I_{11/2}$ relevant states, as well as the ED selection rules for Nd^{3+} ions in each one of the four available cationic lattice sites. According to the observed (σ, π) character for all the transitions of the $^4F_{3/2} \rightarrow {}^4I_{11/2}$ channel (see Fig. 5), the accommodation of Nd^{3+} at the A1 site should be ruled out. Moreover, the occupation of the B2 site should be also ruled out since for this site no polarization dependence is expected (identical spectra should be obtained for σ and π). Thus, only A2 and B1 sites can be the locations for Nd^{3+} ions. All these conclusions are also confirmed by the analysis of the different transitions observed in the polarized absorption spectra.

At this point we postulate that the site A2 is the main site occupied by Nd^{3+} ions in SBN. This assignment is based on the evolution of the Nd:SBN emission through phase transition. As previously reported,[14,23] the Nd^{3+} emission intensity is unchanged when passing through the phase transition and this was interpreted as a consequence of the preservation of the noninversion symmetry in the paraelectric phase (C_{2v}) for the A2 sites. On the other hand, the hypothetical emission of Nd^{3+} ions occupying sites with inversion symmetry in the paraelectric phase, as it is the case of B1 sites (D_{2h} symmetry in the nonpolar state), should be quenched in the paraelectric phase, as reported to occur for Yb^{3+} ions located at B1 and A1 sites.[19] Therefore, the A2 site seems the main occupied site for the Nd^{3+} ions.

TABLE I. Irreducible representations corresponding to the split components for two relevant $^{2S+1}L_J$ states and ED selection rules.

Site (symmetry)	Splitting ($^4F_{3/2}$)	Splitting ($^4I_{11/2}$)	Selection rules
A1 (C_4)	$E_{1/2}+E_{3/2}$	$3E_{1/2}+3E_{3/2}$	$E_{1/2} \leftrightarrow E_{3/2}$ (σ) others (σ, π)
A2 (C_S)	$2E_{1/2}$	$6E_{1/2}$	All (σ, π)
B1 (C_{2v})	$2E_{1/2}$	$6E_{1/2}$	All (σ, π)
B2 (C_1)	$2[2B_{1/2}]$	$6[2B_{1/2}]$	Unpolarized

The preferential location of Nd^{3+} in the A2 cationic site over the octahedral B1 and B2 sites is consistent with considerations on the bond distances observed in the SBN structure. In fact, the Nb-O distances range from 1.92 to 2.03 Å for the B1 site, and from 1.88 to 2.11 Å for the B2 site.[15] On the basis of the well-established set of ionic radii published by Shannon[26] the estimated Nd-O bond distances for trivalent neodymium for coordination number 6 is 2.38 Å. So, it seems evident that Nd^{3+} is too large to be easily accommodated in the B1 and B2 distorted octahedral sites. However, this argument, based only on the crystal lattice parameters, cannot be applied to justify the preferential location of Nd^{3+} in the A2 site over the A1 one. The estimated Nd-O bond distances for trivalent neodymium for coordination number 12 is 2.67 Å (the highest one considered in the ionic radii compilation)[26] and Nd^{3+} ions could fit either the cation-oxygen distances for A2 site (Ba/Sr-O from 2.60 to 3.035 Å) or those of A1 site (Sr-O from 2.54 to 2.919 Å). Nevertheless, the A2 site occupancy revealed from optical spectroscopy will be confirmed by EPR results as will be shown in the next section.

2. Electron paramagnetic resonance

The usual spin-Hamiltonian to account for the EPR lines can be written as

$$H = \beta \vec{B} \hat{g} \vec{S} + \vec{S} \hat{A}^{(i)} \vec{I}^{(i)} \tag{1}$$

where β is the Bohr magneton, $\vec{B}$ the magnetic field, $\hat{g}$ the giromagnetic factor matrix, $\vec{S}$ and $\vec{I}$ the electron and nuclear spins of the paramagnetic center, $\hat{A}$ the hyperfine interaction tensor and the superscript (i) indicates the isotope number. EPR spectra of Nd^{3+} ions deal with transitions involving the lowest Stark energy levels of the $^4I_{9/2}$ ground state. For all the available cationic lattice sites of the SBN crystal, this multiplet splits into five Kramers doublets. However, only the lowest Stark doublet is populated at 10 K (temperature of our experiments) and therefore the system can be described from the point of view of the EPR spectroscopy by a fictitious spin $S=1/2$. Neodymium has three even isotopes ^{142}Nd, ^{144}Nd, and ^{146}Nd with nuclear spins $I=0$ and a total natural abundance of 79.5%, and two odd isotopes ^{143}Nd and ^{145}Nd with nuclear spins $I=7/2$, and natural abundances of 12.2% and 8.3%, respectively. Therefore, the EPR spectrum of Nd^{3+} is expected to be composed of an intense central line, due to the even isotopes, and a hyperfine pattern composed of two sets of $2I+1=8$ lines, for the two odd isotopes, with relative intensities proportional to their natural abundances. Due to the intrinsic disorder of the host mentioned in

TABLE II. Possible Nd^{3+} location in SBN crystals and corresponding g-factor principal values with number of EPR signals which should be observed for a general orientation of the external magnetic field. These different signals are due to magnetic inequivalencies.

Site	Principal g values	Number of different EPR signals (magnetic inequivalencies)
B2:C_1	$g_x \neq g_y \neq g_z$	8
A2:C_s	$g_x \neq g_y \neq g_z$	4
B1:C_{2v}	$g_x \neq g_y \neq g_z$	2
A1:C_4	$g_x = g_y \neq g_z$	2

the previous section, the broadening of the EPR lines in Nd:SBN is such that the hyperfine pattern is not resolved in the EPR spectrum.

For a given paramagnetic center in a single crystal, the g factor is a three by three matrix that reflects the site symmetry of the center. The study of the principal g values as well as the magnetic inequivalencies which appear for a general orientation of the external magnetic field, can give an unambiguous determination of the point site symmetry of the paramagnetic center.[27] In Table II we have considered the four possible locations for the Nd^{3+} ions in the SBN structure with the corresponding relationships between the principal g factor values as well as the number of EPR signals that should be observed for a general orientation of the magnetic field. As we can see in Table II, the four possible sites have different EPR behaviors, which will allow us to conclude on the site symmetry of the Nd^{3+} ions in SBN. The B2, A2, and B1 sites are characterized by three different principal g values with 8, 4, and 2 magnetic inequivalent orientations (magnetic inequivalent sites) for a general orientation of the magnetic field, respectively. The A1 site is an axial site characterized by two different principal g values and two magnetic inequivalent sites for a general magnetic-field orientation.

The determination of the principal g values and the study of the magnetic inequivalencies are obtained from the angular variations of the experimental g factor in three orthogonal crystal planes, e.g., the crystallographic (001), (010), and (100) planes. For example, in the (001) [or (ab)] plane, starting from the a axis, the angular variation of the g factor is given by the following equation:[28]

$$g^2(\theta) = g_{aa}^2 \cos^2(\theta) + g_{bb}^2 \sin^2(\theta) \pm 2g_{ab}^2 \sin(\theta)\cos(\theta) \quad (2)$$

where θ is the angle between the magnetic field and the a axis. From the angular variations of the magnetic field in the three (001), (010), and (100) planes, the following matrix representing the g^2 tensor elements in the (abc) axis system can be generated

$$(g^2) = \begin{pmatrix} g_{aa}^2 & g_{ab}^2 & g_{ac}^2 \\ g_{ab}^2 & g_{bb}^2 & g_{bc}^2 \\ g_{ac}^2 & g_{bc}^2 & g_{cc}^2 \end{pmatrix}_{(abc)} \quad (3)$$

and diagonalization of the (g^2) matrix gives the principal g values.

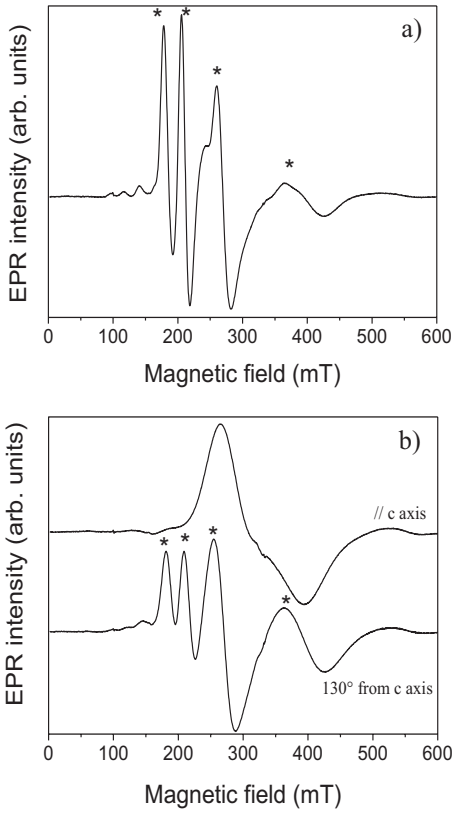

FIG. 6. EPR spectra at 10 K for different geometrical configurations. (a) Magnetic field in the (001) [or (ab)] plane and (b) the magnetic field parallel to c and in a plane containing c. Four different EPR signals indicated by stars are observed corresponding to the same point site symmetry giving four magnetic inequivalencies.

For an arbitrary orientation of the magnetic field, the EPR spectra of Nd^{3+} ions in the SBN host are composed of four types of signals, indicated by stars in Figs. 6(a) and 6(b). When the magnetic field is parallel to the ferroelectric C_4 (c axis) of the structure, these lines are superimposed into one broad line [see Fig. 6(b)]. From the angular variations of the magnetic field in the (ab) plane [Fig. 7(a)] and in a plane perpendicular to (ab) and containing the c axis [Fig. 7(b)], we can observe that these four signals are due to four magnetic inequivalent sites corresponding to only one substitution site. Indeed, in the (ab) plane [Fig. 7(a)], the four types of signals have exactly the same angular variations with the same extrema. This fact indicates that these signals are due to Nd^{3+} ions located in a single site but with different magnetic orientations, in agreement with the results obtained by optical spectroscopy. Moreover, as the angular variations in this plane are not constant in position as a function of the magnetic-field orientation, we can conclude that the site of the Nd^{3+} ions is not axial and that we have $g_x \neq g_y$. From Fig. 7(a), we can thus exclude the A1 site. The only possible sites in the SBN structure which gives four magnetic inequivalent sites is the A2 site, characterized by $g_x \neq g_y \neq g_z$.

In the SBN host, the Nd^{3+} ions in an A2 site are characterized by the following (g^2) matrix:[27]

$$(g^2) = \begin{pmatrix} g_{aa}^2 & g_{ab}^2 & 0 \\ g_{ab}^2 & g_{bb}^2 & 0 \\ 0 & 0 & g_{cc}^2 \end{pmatrix}_{(abc)} \quad (4)$$

If we consider all the symmetry operations of the SBN structure, we have in the (ab) plane four magnetic inequivalent signals with the following g-factor angular variations

$$g^2(\theta) = g_{aa}^2 \cos^2(\theta) + g_{bb}^2 \sin^2(\theta) + 2g_{ab}^2 \sin(\theta)\cos(\theta) \quad (5)$$

$$g^2(\theta) = g_{aa}^2 \cos^2(\theta) + g_{bb}^2 \sin^2(\theta) - 2g_{ab}^2 \sin(\theta)\cos(\theta) \quad (6)$$

$$g^2(\theta) = g_{bb}^2 \cos^2(\theta) + g_{aa}^2 \sin^2(\theta) - 2g_{ab}^2 \sin(\theta)\cos(\theta) \quad (7)$$

$$g^2(\theta) = g_{bb}^2 \cos^2(\theta) + g_{aa}^2 \sin^2(\theta) + 2g_{ab}^2 \sin(\theta)\cos(\theta) \quad (8)$$

In a plane containing the c axis and perpendicular to the (ab) plane, we have also four different EPR signals with the following angular variations:

$$g^2(\theta) = g_1^2 \cos^2(\theta) + g_{cc}^2 \sin^2(\theta) \quad (9)$$

$$g^2(\theta) = g_2^2 \cos^2(\theta) + g_{cc}^2 \sin^2(\theta) \quad (10)$$

$$g^2(\theta) = g_3^2 \cos^2(\theta) + g_{cc}^2 \sin^2(\theta) \quad (11)$$

$$g^2(\theta) = g_4^2 \cos^2(\theta) + g_{cc}^2 \sin^2(\theta) \quad (12)$$

with g_1^2, g_2^2, g_3^2, and g_4^2 given by Eqs. (5)–(8) for a particular value of θ in the (ab) plane.

Equations (5) and (7) and Eqs. (6) and (8) are shifted by 90° corresponding to the C_4-axis symmetry. When the magnetic field is along the a or b axis, Eqs. (5) and (6) and Eqs. (7) and (8) are superimposed, which means that the four signals give only two different ones. This partial magnetic degeneracy allows us to determine the position of these crystallographic axes in our experiments [see Fig. 7(a)]. Equations (9)–(12) for $\theta=\pi/2$ are all identical with $g^2(\frac{\pi}{2})=g_{cc}^2$, which implies that the four magnetic inequivalent signals give only one EPR signal along the c axis, as seen in Figs. 6(b) and 7(b).

For the (ab) plane, Eqs. (5)–(8) are simultaneously used to simulate the angular variations of the four EPR signals. The simulations are shown in Fig. 7(a) (full lines) and give the following g-factor values: $g_{aa}^2=12.1\pm0.1$, $g_{bb}^2=3.9\pm0.1$, and $g_{ab}^2=3.9\pm0.1$. In the plane containing the c axis, Eqs. (9)–(12) are used to simulate the EPR signals and we obtain $g_{cc}^2=3.7\pm0.1$. Thus, diagonalization of the (g^2) matrix gives the following principal g values: $|g_x|=3.7\pm0.1$, $|g_y|=1.5\pm0.1$, and $|g_z|=1.9\pm0.1$

As a conclusion, the EPR study gives $g_x \neq g_y \neq g_z$ with four magnetic inequivalent EPR signals for a general orientation of the magnetic field. The only site for the Nd^{3+} ions that can account for these two observations is the A2 site with C_s point symmetry.

B. Energy levels and crystal field around Nd^{3+} ions

Once the site occupied by the Nd^{3+} ions has been unequivocally determined we are able to estimate the crystal field acting on the Nd^{3+} ions in the A2 sites, i.e., the C_s crystal field parameters. For this purpose we have first used the low-temperature absorption and emission spectra to experimentally determine up to 74 energy levels in the range $0-30\,000\ \text{cm}^{-1}$. These experimental energy levels are listed in Table III. Then these energy levels have been simulated by considering a Hamiltonian $H=H_{\text{FI}}+H_{\text{CF}}$. This Hamiltonian consists in two terms: the free-ion Hamiltonian, H_{FI}, and a crystal field perturbation Hamiltonian, H_{CF}, which represents the crystalline field produced by the host crystal on the Nd^{3+} ions. The free-ion Hamiltonian is given by

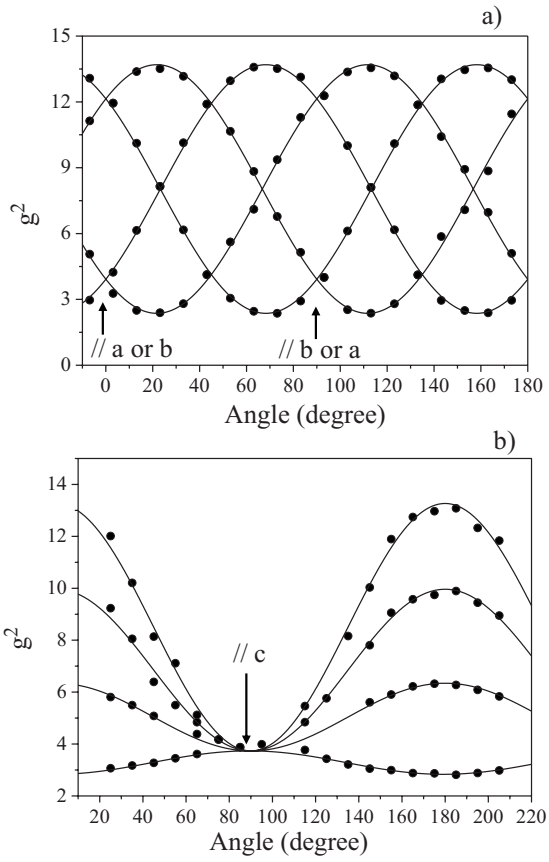

FIG. 7. Experimental and simulated angular variations of g^2 in, (a) the (ab) plane and (b) in a plane perpendicular to (ab) containing c.

$$H_{\text{FI}} = H_0 + \sum_{k=0}^{3} e_k E^K + \zeta A_{SO} + \alpha L(L+1) + \beta G(G_2) + \gamma G(R_7) + \sum_i T^i t_i + \sum_j P^j p_j + \sum_n M^n m_n \quad (13)$$

where H_0 is the spherically symmetric one-electron term of the Hamiltonian, E^k and ζ are the Racah parameters and the spin-orbit coupling constant. α, β, and γ are parameters that take into account two body interactions, while T^2, T^3, T^4, T^6, T^7, and T^8 account for three body interactions. P_j $(j=2,4,6)$ are the electrostatically correlated spin-orbit parameters. The M^n $(n=2,4,6)$ parameters consider the spin-spin and spin-other orbit interactions. All other factors represent the associated angular operators.[29]

TABLE III. Experimental and calculated energy levels of Nd^{3+} in SBN. *E* levels obtained by emission experiments and *A* obtained by absorption experiments. (*) this energy level display a bad fit and was not considered in the root-mean estimation.

$^{2S+1}L_J$ state	Technique	Expt. (cm^{-1})	Calc. (cm^{-1})	Δ (cm^{-1})
$^4I_{9/2}$	*E*	0	13	−13
	E	125	110	15
	E	475	382	93*
	E	581	552	29
	E	648	659	−11
$^4I_{11/2}$	*E*	2087	2079	8
	E	2122	2151	−29
	E	2200	2210	−10
	E	2243	2255	−12
	E	2328	2311	17
	E		2359	
$^4I_{13/2}$	*A*	3965	3998	−33
	A	4000	4059	−59
	A	4078	4110	−32
	A	4146	4170	−24
	A		4254	
	A		4276	
	A		4401	
$^4I_{15/2}$	*A*	5770	5767	3
	A	5886	5873	13
	A	6024	6023	1
	A	6184	6180	4
	A		6312	
	A	6418	6426	−8
	A		6546	
	A	6757	6728	29
$^4F_{3/2}$	*A*	11488	11488	0
	A	11571	11557	14
$^4F_{5/2}$, $^2H(2)_{9/2}$	*A*	12483	12479	4
	A	12522	12534	−12
	A	12549	12556	−7
	A		12608	
	A	12620	12639	−19
	A	12757	12761	−4
	A		12928	
	A	12908	12963	−55
$^4F_{7/2}$, $^4S_{3/2}$	*A*	13389	13389	0
	A		13453	
	A	13512	13534	−22
	A		13644	
	A	13648	13651	−3
	A		13680	
$^4F_{9/2}$	*A*		14687	
	A	14751	14729	22
	A	14797	14788	9
	A		14835	
	A	14848	14862	−14
$^2H_{11/2}$	*A*	15934	15966	−32
	A	15962	15981	−19
	A	15980	15987	−7
	A	16021	16009	12
	A		16063	
	A	16134	16100	34
$^4G_{5/2}$	*A*	17062	17056	6
	A	17114	17146	−32
	A	17156	17210	−54
$^2G(1)_{7/2}$	*A*	17379	17377	2
	A	17437	17408	29
	A	17498	17514	−16
	A		17561	
$^4G_{7/2}$	*A*	18939	18942	−3
	A	19004	18997	7
	A	19088	19108	−20
	A	19164	19171	−7
$^2K_{13/2}$, $^4G_{9/2}$	*A*	19357	19355	2
	A	19451	19425	26
	A	19489	19487	2
	A	19531	19520	11
	A		19560	
	A	19596	19581	15
	A		19687	
	A		19513	
	A		19754	
	A		19815	
	A	19908	19916	−8
	A		19926	
$^2G(1)_{9/2}$,	*A*	20960	20928	32
$^2D(1)_{3/2}$, $^4G_{11/2}$,	*A*	21000	20970	30
$^2K_{15/2}$	*A*	21022	21015	7
	A	21061	21042	19
	A		21112	
	A		21165	
	A	21186	21193	−7
	A	21308	21302	6
	A		21346	
	A		21405	
	A	21505	21493	12
	A		21531	
	A	21612	21606	6
	A		21630	
	A	21687	21682	5
	A	21744	21743	1
	A		21768	

TABLE III. (*Continued.*)

$^{2S+1}L_J$ state	Technique	Expt. (cm^{-1})	Calc. (cm^{-1})	Δ (cm^{-1})
	A		21786	
	A		21845	
	A		21904	
	A	21949	21954	−5
$^2P_{1/2}$	*A*	23272	23245	27
$^2D(1)_{5/2}$	*A*	23759	23788	−29
	A	23855	23847	8
	A	23981	23961	20
$^2P_{3/2}$	*A*	26008	26030	−22
	A	26110	26136	−26
$^4D_{3/2}$, $^4D_{5/2}$	*A*		27774	
	A	27886	27889	−3
	A		27987	
	A	28074	28067	7

The crystalline-field perturbation depends on the local symmetry around the Nd^{3+} ion and it can be described in the frame of the Wybourne formalism.[30] Thus, we now consider that the symmetry around Nd^{3+} ions in SBN is C_S. This symmetry requires the following crystal field parameters: B_0^2, B_0^4, B_0^6, B_2^2, B_2^4, B_4^4, B_2^6, B_4^6, B_6^6, where B_0^2, B_0^4, B_0^6, B_2^2 are real and B_2^4, B_4^4, B_2^6, B_4^6, B_6^6 are complex. As for Ref. 31 B_2^2 is considered real by a proper choice of reference axis system.

Thus, the crystal field Hamiltonian can be written as

$$H_{\mathrm{CF}} = \sum_k B_0^k C_0^k + \sum_{k,q>0} \mathrm{Re}\, B_q^k [C_q^k + C_{-q}^k] + i\, \mathrm{Im}\, B_q^k [C_q^k - C_{-q}^k] \tag{14}$$

with $k=2$, 4, 6, and $q \leq k$.

Once the Hamiltonian has been defined, an iterative process similar to that described in Ref. 32 was used in order to simulate the experimental energy levels with a minimum standard deviation. The simulated energy levels are listed in Table III in comparison with the experimentally obtained energy levels. It can be seen that in the fitting procedure, levels not experimentally detected are obtained. Obviously, the nonobservation of these levels should be due to the large inhomogeneous broadening of the SBN:Nd bands. Except for the experimental energy level at 475 cm^{-1}, it can be seen that there is a reasonably good agreement between the calculated and experimental energy levels, with a root-mean-square deviation of 26 cm^{-1}. The Hamiltonian parameters obtained from this calculation are listed in Table IV.

As a further check to validate our crystal field parameters, the principal g values corresponding to the lowest (0 cm^{-1}) energy level were theoretically estimated using the wave functions corresponding to the Kramers' doublet of the calculated ground-energy level, as described in Ref. 33. In fact, the two wave functions of the ground-state Kramers' doublet are a linear combination of M_J states because of the mixing by nondiagonal crystal field terms. The obtained principal g values are given in Table V. A relatively good agreement is obtained between the experimental and calculated g factor values, despite the low point site symmetry which requires the determination of a high number of crystal field parameters Eq. (14) with only 74 energy levels. Obviously, an improvement would be expected if one could increase the number of experimental energy levels. Moreover, possible local charge compensations could also affect the starting parameters taken in our calculation.

TABLE IV. Hamiltonian parameters for Nd^{3+} in SBN, derived from the analysis defined according to Eqs. (13) and (14).

Parameter	Parameter value (cm^{-1})
E^1	4750
E^2	22.6
E^3	476.8
ζ	865
α	22.5
β	−653
γ	1594
T^2	362.5
T^3	51.9
T^4	83.7
T^6	−313
T^7	366
T^8	464
M^0	1.80
P^2	166
B_0^2	−312
B_0^4	265
B_0^6	−1698
B_2^2	−325
Re B_2^4	−629
Im B_2^4	119
Re B_4^4	737
Im B_4^4	136
Re B_2^6	535
Im B_2^6	−83
Re B_4^6	27.6
Im B_4^6	695
Re B_6^6	580
Im B_6^6	759
N[a]	74
σ [b] (cm^{-1})	26,5

[a]Number of experimental levels included in data fit $n=74$.
[b]Root-mean-square deviation between calculated and experimental energy levels $\sigma=26$, 5 cm^{-1} without considering the level at 475 cm^{-1} (* in Table III).

TABLE V. Experimental and calculated $|g_x|$, $|g_y|$, and $|g_z|$ values for Nd^{3+} in SBN.

	Expt.	Calc.
$\|g_x\|$	3.7	2.9
$\|g_y\|$	1.5	1.6
$\|g_z\|$	1.9	1.8

IV. CONCLUSION AND FINAL REMARKS

In conclusion, the results obtained by polarized optical spectroscopy (including site selective spectroscopy) are consistent with a single location of Nd^{3+} ion in the cationic A2 site. This result contrasts with that previously reported for Yb^{3+} ions in SBN for which no preferential occupation is observed.[20] The different behavior between both ions can be related to their different ionic radii, much smaller for Yb^{3+} ions, which facilitates its accommodation at any of the four possible lattice sites. In the present work the EPR results have confirmed the single location for Nd^{3+} ions and the preservation of the local symmetry (C_s) of the A2 site, which is partially occupied by Sr^{2+} and Ba^{2+} host cations in SBN. Therefore, no evidence has been obtained of local charge compensation. This necessary charge compensation probably occurs at larger distances in comparison to the near neighbor environment around the Nd^{3+} (A2) ions. Finally, a first calculation of the Hamiltonian parameters (considering C_s local symmetry) has been performed for the Nd^{3+} ions in SBN. These conclusive experiments will help to understand the laser and spectroscopic properties of SBN:Nd based optical devices.

ACKNOWLEDGMENTS

This work has been supported by the Spanish Ministry of Science MICINN (Grant No. MAT-2007-64686) and by the Comunidad Autónoma de Madrid (Grant No. CCG07-UAM/MAT-1861). H.L. acknowledges Fundación Carolina for financial support for a research stay in Madrid.

*On leave from Dpto. de Investigación en Física, Universidad de Sonora, P.O. Box 5-088, 83190 Hermosillo, México.
†Deceased.

[1] R. R. Neurgaonkar and W. K. Cory, J. Opt. Soc. Am. B **3**, 274 (1986).
[2] P. V. Lenzo, E. G. Spencer, and A. A. Ballman, Appl. Phys. Lett. **11**, 23 (1967).
[3] M. Goulkov, M. Imlau, T. Granzow, and Th. Woike, J. Appl. Phys. **94**, 4763 (2003).
[4] T. Granzow, Th. Woike, M. Wöhlecke, M. Imlau, and W. Kleemann, Phys. Rev. Lett. **89**, 127601 (2002).
[5] P. Molina, M. O. Ramírez, and L. E. Bausá, Adv. Funct. Mater. **18**, 709 (2008).
[6] J. J. Romero, D. Jaque, J. García Solé, and A. A. Kaminskii, Appl. Phys. Lett. **78**, 1961 (2001).
[7] M. O. Ramírez, P. Molina, and L. E. Bausá, Appl. Phys. B: Lasers Opt. **81**, 827 (2005).
[8] M. O. Ramírez, D. Jaque, L. E. Bausá, J. García Solé, and A. A. Kaminskii, Phys. Rev. Lett. **95**, 267401 (2005).
[9] E. Martín Rodríguez, D. Jaque, J. García Solé, and R. Pankrath, Appl. Phys. Lett. **92**, 181107 (2008).
[10] C. David, T. Granzow, A. Tunyagi, M. Wöhlecke, Th. Woike, K. Betzel, M. Ulex, M. Imlau, and R. Pankrath, Phys. Status Solidi **201**, R49 (2004)
[11] T. Volk, V. Yu. Salobutin, L. I. Ivleva, N. M. Polozkov, R. Pankrath, and M. Wöhlecke, Phys. Solid State **42**, 2129 (2000).
[12] T. Volk, L. Ivleva, P. Lykov, N. Polozkov, V. Salobutin, R. Pankrath, and M. Wöhlecke, Opt. Mater. **18**, 179 (2001).
[13] Ä. Andresen, A.-N. Bahar, D. Conradi, I.-I. Oprea, R. Pankrath, U. Voelker, K. Betzler, M. Wöhlecke, U. Caldiño, E. Martín, D. Jaque, and J. García Solé, Phys. Rev. B **77**, 214102 (2008).
[14] U. Caldiño, P. Molina, M. O. Ramirez, D. Jaque, L. E. Bausá, C. Zaldo, L. Ivleva, M. Bettinelli, and J. García Solé, Ferroelectrics **363**, 150 (2008).
[15] P. B. Jamieson, S. C. Abrahams, and J. L. Bernstein, J. Chem. Phys. **48**, 5048 (1968).
[16] T. Woike, V. Petricek, M. Dusek, N. K. Hansen, P. Fertey, C. Lecomte, A. Arakcheeva, G. Chapuis, M. Imlau, and R. Pankrath, Acta Crystallogr. B **59**, 28 (2003).
[17] T. S. Chernaya, B. A. Maksimov, I. A. Verin, L. I. Ivleva, and V. I. Simonov, Crystallogr. Rep. **42**, 375 (1997).
[18] S. Podlozhenov, H. A. Graetsch, J. Schneider, M. Ulex, M. Wöhlecke, and K. Betzler, Acta Crystallogr. B **62**, 960 (2006).
[19] M. O. Ramírez, L. E. Bausá, A. Speghini, M. Bettinelli, L. Ivleva, and J. García Solé, Phys. Rev. B **73**, 035119 (2006).
[20] M. O. Ramírez, L. E. Bausá, J. García Solé, A. Kaminska, S. Kobyakov, and A. Suchocki, Phys. Rev. B **74**, 174113 (2006).
[21] M. Daldosso, A. Speghini, P. Ghigna, M. de la O. Ramirez, D. Jaque, L. E. Bausá, J. García Solé, and M. Bettinelli, J. Alloys Compd. **451**, 12 (2008).
[22] R. C. Baetzold, Phys. Rev. B **48**, 5789 (1993).
[23] M. O. Ramírez, D. Jaque, L. E. Bausá, J. García Solé, A. Speghini, and M. Bettinelli, Ferroelectrics **337**, 33 (2006).
[24] R. M. Macfarlane, F. Konz, Y. Sun, and R. L. Cone, J. Lumin. **86**, 311 (2000).
[25] J. J. Romero, D. Jaque, L. E. Bausá, A. A. Kaminskii, and J. García Solé, J. Lumin. **87-89**, 877 (2000).
[26] R. D. Shannon, Acta Crystallogr. A **32**, 751 (1976).
[27] J. A. Weil, T. Buch, and J. E. Clapp, Adv. Magn. Reson. **6**, 183 (1973).
[28] F. E. Mabbs and D. Collinson, in *Electron Paramagnetic Resonance of d Transition Metal Compounds* (Elsevier, New York, 1992), Vol. 16.
[29] H. H. Marvin, Phys. Rev. **71**, 102 (1947).
[30] B. G. Wybourne, *Spectroscopic Properties of Rare Earths* (Wiley, New York, 1965).
[31] A. Lupei, E. Antic-Fidancev, G. Aka, D. Vivien, P. Aschehoug, Ph. Goldner, F. Pellé, and L. Gheorghe, Phys. Rev. B **65**, 224518 (2002).
[32] H. Loro, D. Vasquez, G. E. Camarillo, H. del Castillo, I. Camarillo, G. Muñoz, J. C. Flores, A. J. Hernandez, and S. H. Murrieta, Phys. Rev. B **75**, 125405 (2007).
[33] R. S. Rubins, Phys. Rev. B **1**, 139 (1970).